PCCP

Accepted Manuscript

ROYAL SOCIETY OF CHEMISTRY

www.rsc.org/pccp

Journal Name

ARTICLE

Ultrafast spectroscopy, superluminescence and theoretical modeling for a two-photon absorbing fluorene derivative†

Received 00th January 20xx,
Accepted 00th January 20xx

DOI: 10.1039/x0xx00000x

www.rsc.org/

S. A. Kurhuzenkau,[a] A. W. Woodward,[b] S. Yao,[b] K. D. Belfield,[c] Y. O. Shaydyuk,[d] C. Sissa,[a] M. V. Bondar*[d] and A. Painelli*[a]

A comprehensive study of photophysical and photochemical properties of an unsymmetrical fluorene derivative is presented, including linear absorption, fluorescence excitation anisotropy, photochemical stability, steady-state fluorescence, and fluorescence lifetimes in organic solvents of different polarity. Nonlinear optical properties were investigated by Z-scan measurements of degenerate two-photon absorption and femtosecond pump-probe spectroscopy. The strongly fluorescent compound exhibited good photostability, positioning it for use in a number of applications. A dramatic increase in fluorescence intensity along with spectral narrowing was observed under femtosecond pumping, demonstrating amplified spontaneous emission. An extensive set of experimental data are rationalized based on essential state models .

Introduction

Rapid development in photonics, imaging and fabrication techniques, such as two- and multi-photon excitation fluorescence microscopy,[1-3] 3D microfabrication and optical data storage,[4-7] optical power limiting[8] and photodynamic therapy[9] has created a demand for the synthesis and characterization of molecular probes with appropriate characteristics. Effective dyes for two-photon imaging applications for sure have a good two-photon absorptivity in the desired spectral region, typically in the tuning range of Ti:sapphire lasers, but other properties are also in demand. To ensure high-quality images, the dye must show a large fluorescence quantum yield, and high photo- and thermostability,[10] since the image contrast depends on the brightness of the probe and is strongly limited by bleaching.[11] Biocompatibility is another important issue, as well as the possibility to functionalize the dye for targeting specific bio-structures.[12]

Nowadays, design and synthesis of new fluorescent probes for two-photon fluorescence microscopy (2PFM) and other nonlinear optics applications is a developing area with the main target of understanding how chemical structure affects nonlinear optical susceptibility.[9,13] Fluorene-based dyes are widely investigated in this respect.[14,15,16,17] The fluorenyl core provides a rigid flat structural unit with high photostability[13] and acts both as an electron acceptor and as a π-conjugated bridge in either donor-acceptor dyes or in quadrupolar structures, favoring intramolecular charge transfer processes and, hence, enhancing two-photon absorption.[9,13]

Here we present a comprehensive photophysical, photochemical and nonlinear optical characterization of an unsymmetrical D-A-R substituted fluorene, 3,3'-(2-(benzo[d]thiazol-2-yl)-7-(diethylamino)-9H-fluorene-9,9-diyl) dipropanenitrile (**1**), where D is the diethylamino group acting as a good electron-donating unit, R is the benzothiazol unit and A is the fluorene core. Linear spectral properties of **1** were studied in solvents of different polarities. Investigated nonlinear optical properties include two-photon absorption (2PA), excited state absorption and superluminescence emission upon femtosecond excitation. A three state model rationalizes experimental results, shedding light on the role of charge-transfer interactions in the definition of spectral properties. The efficient superluminescence of **1**, its good photostability and high fluorescence quantum yield make this probe an appealing candidate for both two-photon microscopy and organic lasing applications.

Materials and methods

Linear photophysical and photochemical characterization

The molecular structure of **1** is illustrated in Figure 1 and the synthetic procedure is described in Ref. 18. Absorption, steady-state and time-resolved fluorescence measurements in cyclohexane (CHX), toluene (TOL), tetrahydrofuran (THF), dichloromethane (DCM), dimethyl sulfoxide (DMSO), acetonitrile (ACN), and polytetrahydrofuran (pTHF) were

[a] Department of Chemistry, University of Parma, Parco Area delle Scienze 17/A, Parma, 43124, Italy. E-mail: anna.painelli@unipr.it
[b] Department of Chemistry, University of Central Florida, Orlando, FL 32816-2366, United States
[c] College of Science and Liberal Arts, New Jersey Institute of Technology, University Heights, Newark, NJ 07102, United States
[d] Institute of Physics National Academy of Science of Ukraine, Prospect Nauki, 46, Kiev-28, 03028, Ukraine. E-mail: mike_bondar@hotmail.com
†Electronic Supplementary Information (ESI) available: Detailed description of the setup for transient absorption measurements. See DOI: 10.1039/x0xx00000x

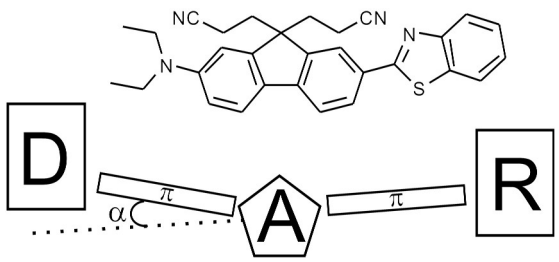

Figure 1. Molecular structure of fluorene derivative **1** and a dye sketch for essential-state modeling (see below)

carried out using a Lambda 650 (Perkin Elmer) spectrophotometer and Fluoromax-3 (Horiba Jobin Yvon) spectrofluorimeter at a room temperature.

Lifetime measurements were performed via time-correlated single photon counting using 403 nm excitation (pulse duration τ_p < 250 ps, 1 MHz repetition rate). Quantum yield measurements were made by a comparative method using fluorescein in 0.1 M NaOH as a standard[19] (Φ_{fl} = 0.92). Steady-state excitation and emission anisotropy spectra were measured and correction was applied for the background signals. All measurements were done in dilute solution (C~20 μM for absorption and C≤2 μM for fluorescence) using spectroscopic-grade solvents.

The photochemical stability of **1** was investigated in air-saturated solvents. We used the Xe-lamp of the spectrofluorimeter (irradiation wavelength λ_{irr}≈400 nm, irradiation intensity I_0≈3.5 mW/cm^2) to illuminate the entire volume of a solution with concentration C≈30 μM in a standard quartz cuvette (1 cm × 1 cm × 3.5 cm). The photostability of **1** was measured in terms of the photochemical decomposition quantum yield, determined from the decrease of optical density of the solution *D(λ,t)* upon illumination:[20]

$$\Phi_{ph} = \frac{N_{mol}}{N_{ph}} \approx \frac{\left(D(\lambda_{\max},0) - D(\lambda_{\max},\tau)\right)N_A}{10^3 \cdot \varepsilon(\lambda_{\max}) \cdot \tau \cdot \int_{\lambda} I(\lambda) \cdot \left(1 - 10^{-D(\lambda,0)}\right) d\lambda}$$

where N_{mol} is the number of photobleached molecules, N_{ph} is the number of absorbed photons, N_A is Avogadro constant, τ is the irradiation time, ε is molar extinction coefficient in M^{-1}cm^{-1} of **1**, and *I(λ)* is the spectral distribution of the excitation irradiance.

2PA, transient absorption, and superluminescence measurements

The degenerate two-photon absorption spectra of **1** in TOL was obtained by an open aperture Z-scan technique described in detail elsewhere.[21] Nonlinear transient absorption spectra of **1**, in the subpicosecond range, were investigated by means of a pump-probe technique[22] using a Mira 900-F (Coherent) femtosecond laser system (ESI†).

The superluminescence of **1** was measured in ACN (dye concentration C≈20 mM) under femtosecond transverse excitation by 400 nm pulses with duration (fwhm) ~140 fs, energy E_p ≤8 μJ/pulse and 1 kHz repetition rate. Sample solution in a standard spectrofluorimetric quartz cuvette was excited with a vertically polarized pump beam. To achieve higher efficiency of light amplification[23] the excitation beam was focused by a cylindrical lens into a 3.0 mm long and 0.15 mm wide stripe. The fluorescence emission, collected from the side surface of the cuvette by a high-aperture lens, was sent to the spectrometer. The superluminescence emission intensity is unaffected by small rotation or tilting of the cuvette, proving the absence of laser feedback due to the reflections from the cell walls.

Results and discussion

Linear photophysical and photochemical studies

Linear absorption, emission and excitation anisotropy spectra, and main photophysical and photochemical parameters of **1** are summarized in Figure 2 and Table 1.

The marginal absorption solvatochromism of **1** and its large fluorescence solvatochromism suggest that **1** is weakly polar in the ground state, but acquires a large polarity upon photoexcitation. The Stokes shift shows an approximately linear dependence on the solvent orientation polarizability $\Delta f = \frac{\varepsilon-1}{2\varepsilon+1} - \frac{n^2-1}{2n^2+1}$ (Figure 2b), in good agreement with Lippert equation,[24] pointing to the absence of specific solute-solvent interactions and to a marginal variation of the chromophore polarity in the different solvents.[25] This result is also supported by the marginal solvent dependence of the oscillator strength (see Table 1).

The dye shows a very high fluorescence quantum yield (Φ_{fl} ~ 0.80-0.96) and single-exponential decay in all solvents. The radiative lifetimes estimated based on the Strickler-Berg relation[26] are slightly overestimated with respect to the experimental radiative lifetimes $\tau_{rad} = \tau_{fl}/\Phi_{fl}$ (see Table 2), and show a smooth increase with solvent polarity that can be ascribed to the red-shift of the fluorescence.

A very low value (<0.06) is measured for the fluorescence excitation anisotropy in low-viscosity solvents (see Figure 2c), due to the fast rotation of the dye before emission. The inverse excitation anisotropy shows a linear dependence vs. the solvent viscosity η (see Figure 2d) in agreement with the equation:[24] $\frac{1}{r} = \frac{1}{r_0} + \frac{kT}{r_0 V}\frac{\tau_{fl}}{\eta}$ (where *k* is the Boltzmann constant and *T* is temperature), suggesting that *V,* the effective rotational volume of the molecule, and r_0, the fundamental anisotropy, are essentially solvent independent.

Table 1. Main photophysical and photochemical parameters: λ_{max}^{abs} and λ_{max}^{fl} – absorption and emission wavelengths maxima, ε_{max} – extinction coefficient at λ_{max}^{abs}; *f* – oscillator strength; Φ_{fl} – fluorescence quantum yield; τ_{fl} – fluorescence lifetime; Φ_{ph} – photodecomposition quantum yield.

Solvent	CHX	TOL	THF	DCM	ACN	DMSO
λ_{max}^{abs}, nm	383	394	398	399	397	407
λ_{max}^{fl}, nm	439	463	491	495	534	545
$\varepsilon_{max}\cdot10^{-3}$, M^{-1} cm^{-1}	53	46	44	48	46	47
f	0.88	0.81	0.81	0.88	0.88	0.90
Φ_{fl}, %	96	95	86	95	80	88
τ_{fl}, ns	1.4	1.6	1.9	2.0	2.4	2.4
Φ_{ph}, 10^{-5}	5.4	2.3	0.9	4.1	100	

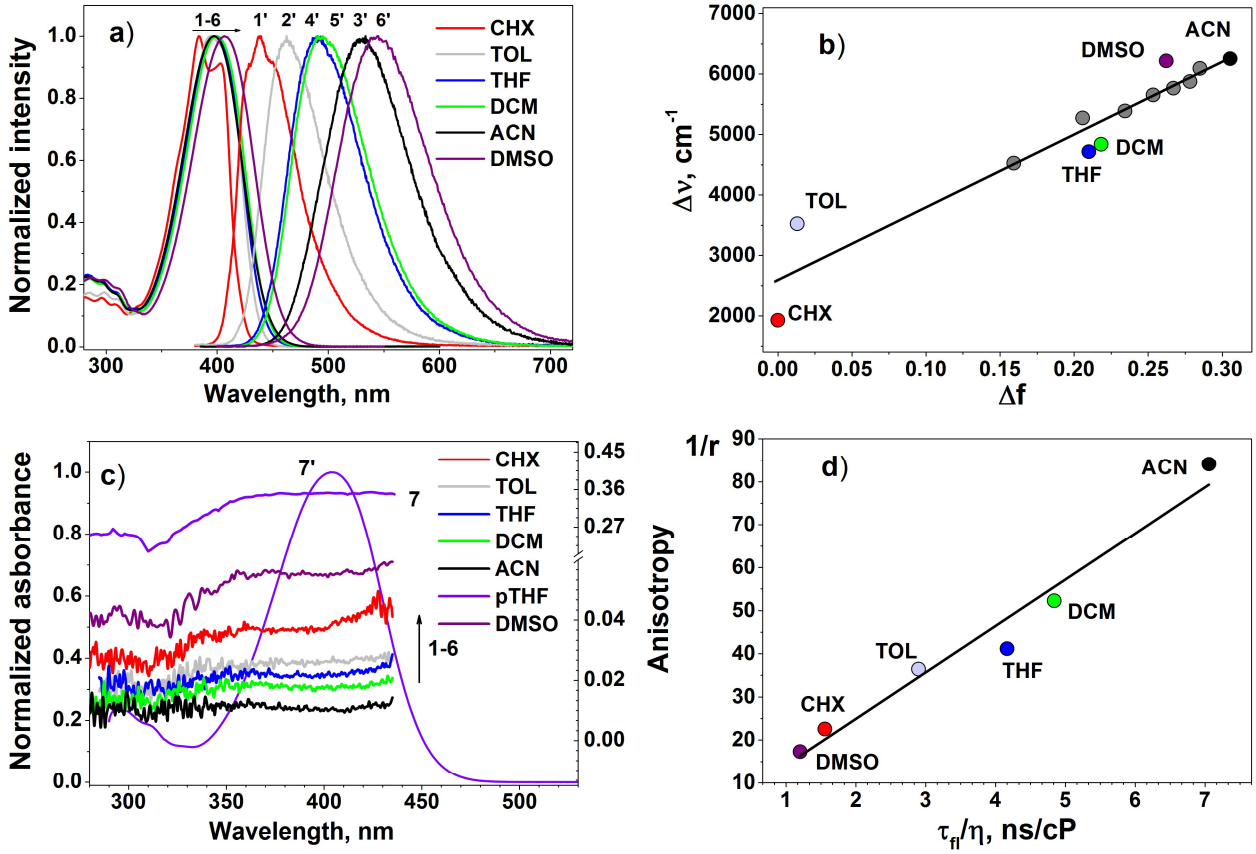

Figure 2. (a) Normalized linear absorption (1-6) and emission (1'-6') of **1** in CHX (1,1'), TOL (2,2'), ACN (3,3'), THF (4,4'), DCM (5,5') and DMSO (6,6'). (b) Lippert plot for **1**. Grey circles represent Stokes shift of **1** measured in ACN-TOL mixtures. (c) Absorption spectra of **1** in pTHF (7') and excitation anisotropy in ACN (1), DCM (2), THF (3), TOL (4), CHX (5), DMSO (6) and pTHF (7). Please notice the scale break in the anisotropy scale on the right axis. (d) Dependence of the inverse fluorescence anisotropy, *1/r,* plotted against the ratio of the fluorescence lifetime over the solvent viscosity, τ_{fl}/η.

In highly viscous polytetrahydrofuran (pTHF) the molecular rotation is hindered and steady state anisotropy gives information on the angle θ between emission and absorption transition dipole moments, $r \approx r_0 = \frac{3cos^2\theta-1}{5}$. In the spectral region corresponding to the lowest energy absorption band, the anisotropy r~0.35 approaches the limiting value 0.4 for parallel absorption and emission dipoles.[24] At higher energy, the anisotropy decreases and a dip is observed near 300 nm with r~0.21, ascribed to an electronic transition whose transition dipole moment makes an angle θ~34° with respect to the emission transition dipole moment.

The photodecomposition quantum yield, Φ_{ph}, measuring the number of photobleached molecules per number of absorbed photons, offers a reliable estimate of the molecular photostability.[20] Φ_{ph} represents an absolute estimate of the molecular photostability (that of course may strongly depend on the surrounding medium) to be contrasted with relative stability estimates more commonly found in literature[11,27,28] that are highly dependent on experimental conditions. Dye **1** exhibited good photostability, with Φ_{ph} in range of 10^{-5} (see Table 1), except for ACN where Φ_{ph} increased by 2 orders of magnitude. The lowest values of Φ_{ph} are approaching the photostability of typical laser dyes, such as Rhodamine 6G with photobleaching yields in the range $0.3\cdot10^{-6}$-$1.5\cdot10^{-5}$, depending on the solvent.[29,30] The low values of Φ_{ph} obtained in solvents of low and moderate polarity along with high fluorescence quantum yield makes **1** interesting for bioimaging applications. Just as an example, in THF a single dye molecule can undergo up to ~10^5 excitation-emission cycles before photobleaching.

Table 2. Transition dipole moment estimated from the oscillator strength for the lowest energy transition. The radiative lifetime τ_{rad} and the Strickler-Berg radiative lifetime, τ_{rad}^{SB}

Solvent	CHX	TOL	THF	DCM	ACN	DMSO
μ_{01}, D	8.5	8.3	8.3	8.7	8.6	8.7
τ_{rad}, ns	2.2	2.5	3.2	3.0	4.0	3.5
τ_{rad}^{SB}, ns	1.5	1.7	2.2	2.1	3.0	2.7

Transient absorption, 2PA and superluminescence of 1

Figure 3 shows transient changes in absorption (ΔD) for **1** in TOL and ACN upon photoexcitation at 400 nm (roughly corresponding to the maximum of the lowest absorption). In the absence of photoinduced chemical reactions or photoisomerization processes, the nature of the kinetic curves is determined by 3 processes: ground-state bleaching (or saturable absorption), stimulated emission (SE, gain), and

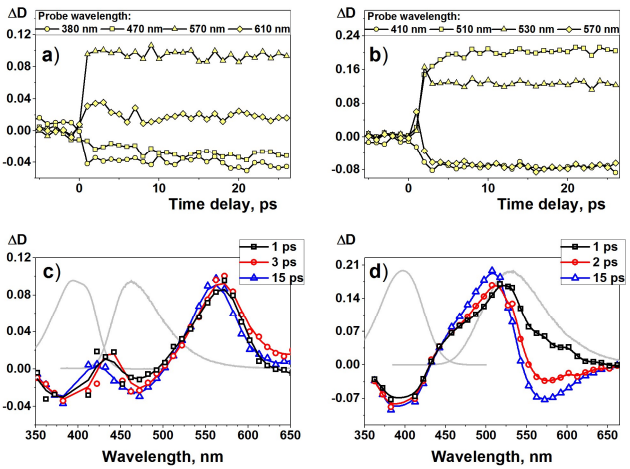

Figure 3. Transient absorption of **1**. Temporal dependencies of ΔD(Δt) and spectral dependencies of ΔD(λ_{probe}) of **1** in TOL (a,c) and in ACN (b,d). The solid curves in (c) and (d) are stationary absorption and fluorescence of **1** in TOL and ACN, respectively.

excited state absorption (ESA).[22] Ground state bleaching and stimulated emission results in negative values of ΔD, while excited state absorption contributes to positive ΔD signals.

The transient absorption spectra of **1** in nonpolar TOL recorded at different time delays (Figure 3) reveal bleaching near 400 nm, due to the depopulation of the ground state of **1** and strong ESA at 570 nm. Moreover, weak SE, partly superimposed with ESA, may be seen in the region of the steady-state fluorescence. The transient absorption signals appear within the instrumental response time and do not show any major subsequent dynamics, apart from relaxation in the nanosecond time scale, in line with the lifetimes of the S_1 state. Accordingly, the dynamic processes following ultrafast photoexcitation, are completed within the first 500 fs.[24]

In the polar ACN solvent a slightly more complex excited state dynamics was observed. The ground-state bleaching signal appeared at the same position and followed the same decay dynamics as observed in toluene. The ESA peak instead is centered around 530 nm at early time but undergoes a blue-shift, reaching ~515 nm after 3 ps. Spectral narrowing accompanied this shift. Similar information is obtained from the ΔD(Δt) traces in Figure 3. The signal evolution fits well with a monoexponential decay with lifetime ~2 ps. This evolution is clearly due to solvent relaxation.[31] Indeed, as demonstrated by the solvatochromic behavior of the dye, upon photoexcitation the molecular polarity markedly increases. Accordingly, after photoexcitation in polar solvents a reorganization of the solvent around the solute takes place, corresponding to a slow motion typically seen in the ps time-window. The solvent relaxes around the photoexcited molecules, stabilizing the excited state, resulting in a blue-shift of the ESA signal, in line with the large Stokes-shift observed in steady state spectra.[32,33] Concomitantly, the SE signal, initially masked by the superimposed ESA, moved to the red, becoming well visible at ~2 ps as a negative peak at 570 nm and then remaining constant within the experimental time window. The optical gain of **1** in polar solvent could be utilized for exploiting superluminescence and lasing phenomena.

The degenerate 2PA spectrum of **1** was recorded by an open aperture Z-scan technique over a broad spectral range. The 2PA spectrum in Figure 4 shows two well-defined bands at 780 and 620 nm with maximum 2PA cross-sections of 47 and 65 GM, respectively. The efficiency of 2PA in **1** in 600-900 nm range is somewhat smaller compared to the other small unsymmetrical fluorene derivatives, exhibiting 2PA cross-sections of 100-300 GM,[15,34] though it is comparable with maximum 2PA cross-sections of fluorescein (65 GM) and its analogue Alexa 488 dye (~90 GM).[35,36]

The almost perfect overlap of the lowest energy one-photon (1PA) and 2PA bands suggests that the same state, S_1, is responsible for the two features, as expected for a unsymmetrical dye.[37,15] The second peak occurs instead close to the dip in the fluorescence excitation anisotropy, where the 1PA intensity is very low. This suggests a different mechanism for the 2PA intensity of the two peaks: according to the standard sum over state treatment of 2PA,[38] the 2PA intensity of the lowest energy peak has a large contribution from the so-called dipolar term, being proportional to the product of the squared transition dipole moment μ_{01} and the squared mesomeric dipole moment $|\mu_{01}|^2|\mu_{11}-\mu_{00}|^2$, where μ_{11} and μ_{00} are the permanent dipole moments in the first excited state and the ground state, respectively. The dipolar contribution to the 2PA intensity of the second peak is instead negligible. Since the corresponding transition dipole moment from the ground state is negligible the so-called three-state T-term must play the major role.

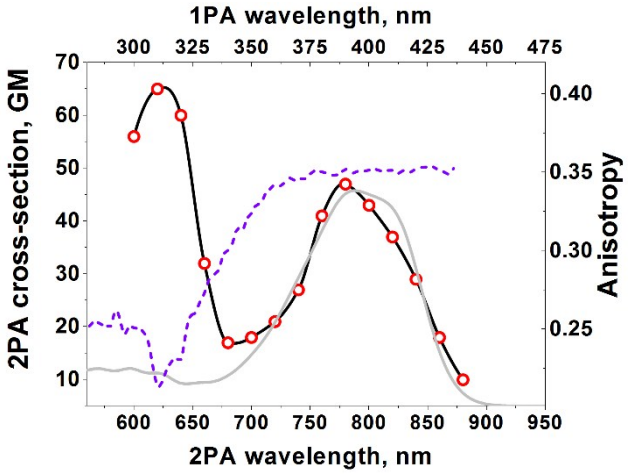

Figure 4. Normalized one-photon (solid line) and two-photon (line plus circles) absorption spectra of **1** in TOL and excitation anisotropy spectra of **1** in pTHF (dashed line).

High fluorescence quantum yield and good photostability together with a sizable 2PA cross-section δ_{2PA} yield a figure of merit[39] $F_M = \Phi \cdot \delta_{2PA}/\Phi_{ph} \sim 6 \cdot 10^6$ GM, similar to other commonly used fluorescent labels, suggesting that **1** can be conveniently used for two-photon fluorescence imaging applications.[16,40]

The signal amplification (gain, ΔD < 0) observed in ACN solution in the 540-620 nm spectral window suggests examining the superluminescent properties the of the dye in this solvent.

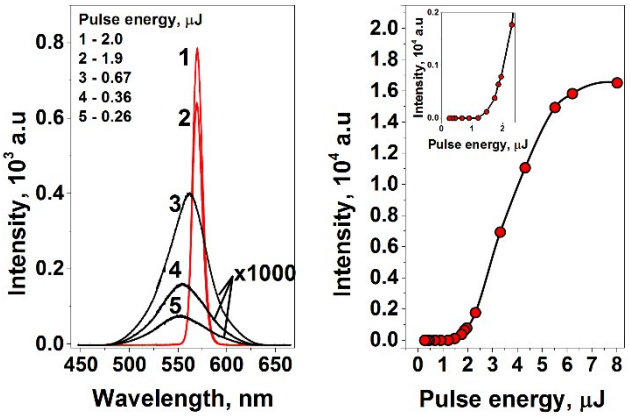

Figure 5. Left: spontaneous and superluminescence emission of **1** in ACN. Right: emission intensity (measured at the band maximum) dependence on pulse energy. The inset is an enlargement of the initial portion of the same graph.

In spite of a comparatively low photostability of **1** in ACN, it is enough as to guarantee marginal decomposition in the time-scale of the experiment, as verified by the lack of decay in the emission intensity.

Emission spectra of **1** under excitation by ultrashort pulses of different energy and the dependence of the maximum emission intensity on the pulse energy are displayed in Figure 5. For weak excitation pulses, broad and structureless emission spectra were observed. The slight red-shift observed with respect to emission spectra in Figure 2 is ascribed to reabsorption effects in the highly concentrated solution used for superluminescence experiments

For stronger pulses (~1 μJ/pulse and above) the emission intensity grows approximately exponentially and reaches saturation under pumping with a pulse energy of 6-8 μJ. This fast signal saturation can be explained due to the thermo-optical effect: relatively high pump power causes local heating in the gain medium resulting in increased beam divergence, so that part of the emission misses the detector. The intensity growth of the emission was accompanied by a dramatic narrowing of the spectra. FWHM of **1** in ACN emission reduces from 90 nm (see Figure 2) to ≈10 nm at the pump energy of 1.5 μJ/pulse (330 μJ·cm^{-2}). The obtained value of the superluminescence threshold and the observed spectral width are typical for laser dyes.[40-44]

Theoretical modeling

Linear absorption spectra of **1** (Figure 2) are clearly dominated by the peak at ~400 nm, with a much weaker and broader absorption around 290 nm. The 2PA spectrum shows a first peak superimposed with the intense 1PA band, and a second, more intense feature at ~310 nm, approximately in the same position where a dip in the fluorescence excitation anisotropy is observed. The presence of two bands in both 1PA and 2PA spectra with reversed intensity ratios immediately suggest to model **1** as an asymmetric quadrupolar dye, in line with its chemical structure, D-A-R (Figure 1). Models for asymmetric quadrupolar dyes have already been discussed,[45-47] here we adopt the same model described in ref. 45, slightly modified to account for the non-collinearity of the two molecular arms, as needed to account for the anisotropy dip.

Shortly, we describe the electronic structure based on three diabatic states $|N\rangle$=DAR, $|Z_L\rangle$=D$^+$A$^-$R and $|Z_R\rangle$=DA$^-$R$^+$, corresponding to the main resonating structures of **1**. As sketched in Figure 6c, four parameters are needed to describe the electronic Hamiltonian, $2\eta_{L/R}$ measuring the energy to transfer an electron towards A from D (L) and R (R), and $\tau_{L/R}$, the corresponding hopping integrals. The diagonalization of the resulting Hamiltonian matrix leads to three adiabatic states: the ground state, $|G\rangle$, and two excited states, $|E_1\rangle$ and $|E_2\rangle$. To calculate optical spectra the dipole moment operator must be defined. In the chosen diabatic basis, the dipole moment operator is assumed diagonal and we neglect the dipole moment of $|N\rangle$, with respect to the dipole moments $\mu_{L/R}$ and of the two charge-separated structures, $|Z_{L/R}\rangle$. The two dipole moments point in opposite directions and are not collinear, but make an angle α, as sketched in Figure 1. For linear and symmetric molecules, mutual selection rules apply and the first excited state is only 1PA active, while the second state is active in 2PA. Our dye is unsymmetrical and slightly bent, justifying the observation of the same bands both in 1PA and 2PA, with inverse intensities ratios.

To address spectral band-shapes and solvatochromism the model must be extended to account for the coupling of electronic states to molecular vibrations and for polar solvation. As for molecular vibrations, we introduce two vibrational modes, one for each molecular arm. The two modes are set as harmonic, with frequency ω (indeed, in view of the asymmetry of the molecule two different frequencies could be defined for each mode, but this has just minor effects on electronic spectra) and relaxation energies ε_L and ε_R, measuring the energy gained upon relaxation along either coordinate following the DAR →D$^+$A$^-$R and DAR →DA$^-$R$^+$ processes, respectively.

To account for polar solvation, we introduce the reaction field, ***F***, generated by the reorientation of the permanent dipole moments of polar solvent molecules around the solute. In the simplest approximation, i.e. describing the solvent as a continuum dielectric medium with elastic response, ***F*** enters the model as an effective harmonic coordinate, with negligible frequency. The solvent relaxation energy, ε_{or}, vanishes in non-polar solvents and increases with solvent polarity. In planar bent molecules only the two components of the electric field in the molecular plane F_x and F_y are relevant, while the perpendicular component, F_z is irrelevant as it does not affect molecular properties.

The ***F*** dynamics is very slow if compared with either molecular vibrations or electrons dynamics. We therefore treat ***F*** as a classical variable, and diagonalize the molecular Hamiltonian for fixed ***F*** values. The molecular Hamiltonian itself describes the coupled electronic and vibrational motion and, to properly describe excited states, we resort to a numerically exact diagonalization of the non-adiabatic Hamiltonian as described elsewhere.[45] Once exact non-adiabatic eigenstates are obtained, we can calculate the matrix elements of the dipole operator as entering sum-over-state

expressions for linear and nonlinear optical spectra.[45,48] The only additional parameter in the calculation of optical spectra is the intrinsic line width associated to vibronic states that we fix to a constant value γ. The calculations are repeated on a grid of (F_x, F_y) values and the spectra are calculated by summing up the contributions from different points in the grid, weighting each contribution by the relevant Boltzmann distribution. In more physical terms, inhomogeneous broadening due to polar solvents are accounted for calculating solution spectra as sum of the contributions from a collection of molecules, each one experiencing a slightly different reaction field, with a distribution governed by thermal energy average. For linear and nonlinear absorption processes, the Boltzmann distribution is calculated on the basis of the ground state energy, while for fluorescence it refers to the energy of the fluorescent state. A slightly more delicate issue concerns fluorescence anisotropy in liquid solution, where both distributions enter, as discussed in ref. 49 and 50.

Figure 6 collects calculated spectra using molecular model parameters in Table 3. We discuss results relevant to a subset of solvents with different polarity but comparable refractive index, CHX, TOL, DCM and DMSO, as to minimize the effects due to the electronic solvent polarizability.[51] We set γ=0.08 eV as the intrinsic linewidth of the vibronic line for all solvents: inhomogeneous broadening effects that very clearly show up in absorption and fluorescence spectra are fully accounted for by the adopted model, spectral bandshapes are not adjusted by hand. Indeed the only parameter that is changed to account for the increasing solvent polarity is the solvent relaxation energy, ε_{or}, that vanishes in the non-polar solvent CHX and increases up to 0.6 in DMSO. To reproduce the anisotropy spectrum in pTHF we fixed the same ε_{or} as in DCM, and adjusted the molecular bending angle α=10° (see Figure 1 and Figure S2, ESI†). Small variations of the angle around this value do not appreciably affect other spectral properties apart from anisotropy. Calculated fluorescence anisotropy is in good agreement with experimental results, confirming that the model captures the different alignment of transition dipole moments for the two observed transitions (a scheme of calculated transition dipole moments is reported in Figure S3, ESI†).

Table 3. Molecular model parameters for **1**.

η_L, eV	η_R, eV	τ_L, eV	τ_R, eV	ε_L, eV	ε_R, eV	ω, eV	μ_L, D	μ_R, D
1.2	1.7	1.1	0.8	0.45	0.55	0.17	20	14

The calculated 2PA spectrum compares very well with the experimental spectrum in terms of band-positions and shape. The intensity ratio ~0.6 is calculated between the lowest and highest energy 2PA peaks is reasonable agreement with the experimental 0.7 value. The calculated absolute 2PA intensity is overestimated by a factor of 2, that could be easily improved by accounting for the correction of the calculated 2PA spectrum by the inverse squared refractive index of the solvent (n_{tol}=1.4968).

The very good agreement between calculated and

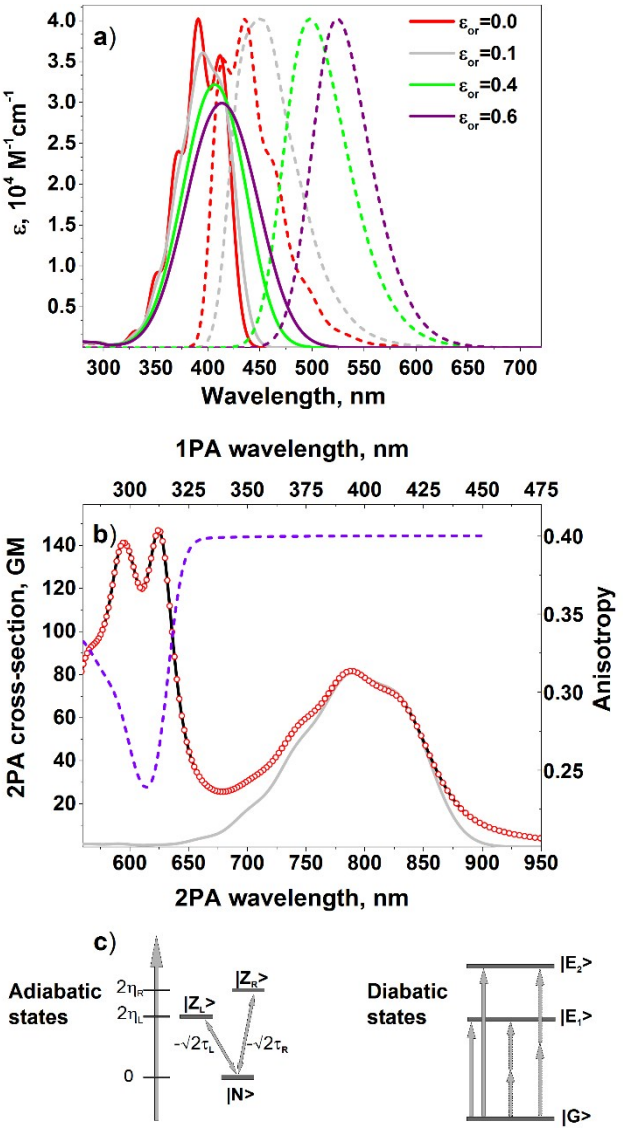

Figure 6. (a) Calculated absorption (continuous lines) and emission (dashed lines) spectra of **1**, using model parameters in Table 3. The solvent relaxation energy in the legend is set to mimic, in increasing order of polarity, the solvents CHX, TOL, DCM and DMSO. (b) 1PA (continuous line) and 2PA (open circles) spectra calculated for ε_{or}=0.1 eV, mimicking TOL. Fluorescence excitation spectra are calculated setting ε_{or}=0.4 eV, to mimic the polarity of pTHF. (c) A sketch of electronic states in the adopted essential state model. Diabatic states corresponds to the basis states, for which model parameters are defined. Adiabatic states, obtained from the diagonalization of the electronic Hamiltonian, are those relevant to spectroscopy.

experimental spectra gives us confidence on the proposed model and suggests using the model to better understand the complex spectroscopic behavior of **1**. With $\eta_L<\eta_R$ the D group is a stronger donor than R. Accordingly, the ground state charge distribution estimated in the non-polar solvent is $D^{+0.13}A^{-0.13}R$ with a permanent dipole moment of ~2 Debye, along the molecular axis. In the fluorescent state the dipole moment increases to ~15 Debye, according to a charge distribution $D^{+0.79}A^{-0.86}R^{+0.07}$. Indeed the calculated charge distribution does not change appreciably in polar solvents, apart from a slight decrease of the dipole moment in the relaxed excited state. Quite interestingly, as long as we limit attention to the lowest excited state, $|E_1\rangle$, the dye approximately behaves as a simple

polar DA dye, the R moiety being almost silent. The relevant solvatochromism is indeed that of a largely neutral dye, characterized by a large mesomeric dipole moment. The same two-state model can also account for the observation of a 2PA band superimposed with the 1PA band (even if the relevant intensity would be largely overestimated).

However, to model the second intense 2PA peak one must account for the active role of R: the charge distribution calculated for the state responsible for the second 2PA peak ($|E_2\rangle$, selected as the state with the largest transition dipole moment from the first excited state) is $D^{+0.41}A^{-0.89}R^{+0.48}$, corresponding to a largely quadrupolar state, with a very small permanent dipole moment, amounting to ~2 Debye in the opposite direction with respect to the ground state dipole moment. The marginal difference of polarity of this state with respect to the ground state (at least three times smaller than for the 1PA state) explains the observation of a fairly narrow 2PA feature with well resolved vibronic structure also for finite ε_{or} values.

Conclusions

Comprehensive analysis of photochemical and linear and nonlinear optical properties of a DAR fluorenyl-core dye in different media is presented. One-photon absorption spectra are almost solvent-independent, while fluorescence spectra show a marked red-shift in polar solvents, with a Stokes shift up to 140 nm in strongly polar solvents (e.g., ACN and DMSO). High fluorescence quantum yield (0.80-0.96) and monoexponential fluorescence decay with lifetimes of 1.4-2.4 ns along with high photochemical stability ($\Phi_{ph} \sim 10^{-5}$) were characteristic of **1**.

Excited states absorption of **1** was investigated by femtosecond pump-probe spectroscopy over wide spectral range. In nonpolar TOL all relaxation processes were completed within 500 fs after photoexcitation. However, in ACN a slower solvent relaxation occurred in the ps time-frame. After the solvent relaxation was over a strong gain in the fluorescence band (at ≈ 570 nm) was observed, resulting in efficient superluminescent behavior under femtosecond transverse pumping.

The degenerate 2PA spectra of **1** in TOL was investigated over a broad spectral range, observing two bands with maximum values of 2PA cross sections of ≈ 47 and 65 GM, at 780 and 620 nm, respectively. The lowest energy band was superimposed with the 1PA band, pointing to the same origin of the two transitions, as expected for a non-symmetric dye. The second 2PA band instead falls in a region where the 1PA spectrum is very weak, suggesting a quadrupolar nature of the corresponding state. This intuition is fully consistent with the results of an essential state model for the dye, that described 1 as a bent DAR structure.

This work provides valuable information on photophysical properties of the fluorene based dye **1,** that is useful for the development of bright and stable probes for nonlinear optical applications.

Acknowledgments

The research leading to these results has received funding from the People Programme (Marie Curie Actions) of the European Union's Seventh Framework Programme FP7/2007-2013 under REA grant agreement n. 607721 (Nano2Fun). MVB wishes to acknowledge support from the National Academy of Sciences of Ukraine (grant VC-157) while KDB acknowledges support from the National Science Foundation (CBET-1517273). AP acknowledges support from Italian Ministry of Education and Research MIUR (PRIN 2012T9XHH7).

MVB, YOS and SAK acknowledge the Femtosecond Laser Complex of the Institute of Physics of the National Academy of Sciences of Ukraine for the hardware support

References

1 C. D. Andrade, C. O. Yanez, M. A. Qaddoura, X. Wang, C. L. Arnett, S. A. Coombs, J. Yu, R. Bassiouni, M. V. Bondar and K. D. Belfield, *J. Fluoresc.,* 2011, **21**, 1223–1230.
2 X. Wang, A. R. Morales, T. Urakami, L. Zhang, M. V. Bondar, M. Komatsu and K. D. Belfield, *Bioconjugate Chem.,* 2011, **22**, 1438–1450.
3 K. J. König, *J. Microsc.,* 2000, **200**, 83–104.
4 K. Kurselis, R. Kiyan, V. N. Bagratashvili, V. K. Popov and B. N. Chichkov, *Opt. Express.,* 2013, **21**, 31029–31035.
5 L. Yang, A. El-Tamer, U. Hinze, J. Li, Y. Hu, W. Huang, J. Chu and B. N. Chichkov, *Appl. Phys. Lett.,* 2014, **105**, 041110.
6 C. O. Yanez, C. D. Andrade, S. Yao, G. Luchita, M. V. Bondar and K. D. Belfield, *Appl. Mater. Interf.,* 2009, **1**, 2219–2229.
7 C. C. Corredor, Z. L. Huang, K. D. Belfield, A. R. Morales and M. V. Bondar, *Chem. Mater.,* 2007, **19**, 5165–5173.
8 Y. Bretonnière and C. Andraud, in *Photosensitizers in Medicine, Environment, and Security*, ed. T. Nyokong and V. Ahsen, Springer: Dordrecht, Netherlands, 2012, 619–654.
9 M. Pawlicki, H. A. Collins, R. G. Denning and H. L. Anderson, *Angew. Chem., Int. Ed.,* 2009, **48**, 3244–3266.
10 M. Oheim, D. J. Michael, M. Geisbauer, D. Madsen, and R. H. Chow, *Adv. Drug. Deliv. Rev.,* 2006, **58**, 788–808.
11 G.H. Patterson and D. W. Piston, *Biophys. J.,* 2000, **78**, 2159–2162.
12 C. O. Yanez, A. R. Morales, X. Yue, T. Urakami, M. Komatsu, T. A. H. Järvinen and K. D. Belfield, *PLoS ONE,* 2013, **8**, e67559.
13 F. Terenziani, C. Katan, E. Badaeva, S. Tretiak and M. Blanchard-Desce, *Adv. Mater.,* 2008, **20**, 4641–4678.
14 C. D. Andrade, C. O. Yanez, L. Rodriguez and K. D. Belfield, *J. Org. Chem.,* 2010, **75**, 3975–3982.
15 K. D. Belfield, M. V. Bondar, F. E. Hernandez, O. V. Przhonska and S. Yao, *J. Phys. Chem. B,* 2007, **111**, 12723–12729.
16 S. Yao and K. D.Belfield, *Eur. J. Org. Chem.,* 2012, **17**, 3199–3217.
17 I. V. Kurdyukova and A. A. Ishchenko, *Russ. Chem. Rev.,* 2012, **81**, 258–290.
18 S. Yao, K. J. Schafer-Hales and K. D. Belfield, *Org. Lett.,* 2007, **9**, 5645–5648.
19 D. Magde, R. Wong and P. G. Seybold, *Photochem. Photobiol.*, 2002, **75**, 327–334.
20 C. C. Corredor, K. D. Belfield, M. V. Bondar, O. V. Przhonska, and S. Yao*, J. Photochem. Photobiol. A,* 2006, **184**, 105–112.
21 M. Sheik-Bahae, A. A. Said, T. H. Wei, D. J. Hagan and E. W. Van Stryland, *IEEE J. Quantum Elect.*, 1990, **26**, 760–769.
22 R. Berera, R. van Grondelle and J. T. M. Kennis, *Photosynth. Res.*, 2009, **101**, 105–118.
23 O. Svelto, *Principles of Lasers*, Springer: New York, USA, 5th ed., 2010.

24 J. R. Lakowicz, *Principles of fluorescence spectroscopy*, Springer: New York, USA, 3rd ed., 2006.
25 B. Boldrini, E. Cavalli, A. Painelli and F. Terenziani, J. *Phys. Chem. A,* 2002, **106**, 6286–6294.
26 S. J. Strickler and R. A. Berg, *J. Chem. Phys.,* 1962, **37**, 814–822.
27 T. Jokic, S. M. Borisov, R. Saf, D. A. Nielsen, M. Kühl and I. Klimant, *Anal. Chem.,* 2012, **84**, 6723–6730.
28 S. Zhang, T. Wu, J. Fan, Z. Li, N. Jiang, J. Wang, B. Dou, S. Sun, F. Song and X. Peng, *Org. Biomol. Chem.,* 2013, **11**, 555–558.
29 C. Eggeling, J. Widengren, R. Rigler and C. A. M. Seidel in *Applied fluorescence in chemistry, biology and medicine*, ed. W. Rettig, B. Strehmel, M. Schrader and H. Seifert, Springer, Berlin, 1999, 193–240
30 I. Rosenthal, *Opt. Commun.,* 1978, **24**, 164-166.
31 F. Terenziani and A. Painelli, *Chem. Phys.,* 2003, **295**, 35–46.
32 D. Sharma, J. Leonard and S. Haacke, *Chem. Phys. Lett.,* 2010, **489**, 99–102.
33 A. Painelli and F. Terenziani, *Synthetic Met.*, 2001, **124**, 171–173.
34 K. D. Belfield, M. V. Bondar, F. E. Hernandez, A. E. Masunov, I. A. Mikhailov, A. R. Morales, O. V. Przhonska and S. Yao, *J. Phys. Chem. C*, 2009, **11**, 4706–4711.
35 N. S. Makarov, M. Drobizhev and A. Rebane, *Opt. Express*, 2008, **16**, 4029–4047.
36 C. Xu and W. R. Zipfel, *Cold Spring Harb. Protoc.,* 2015, **3**, 250–258.
37 K. D. Belfield, M. V. Bondar, A. R. Morales, X. Yue, G. Luchita, O. V. Przhonska and O. D. Kachkovsky, *ChemPhysChem.,* 2012, **13**, 3481-3491.
38 D. Beljonne, W. Wenseleers, E. Zojer, Z. Shuai, H. Vogel, S. J. K. Pond, J. W. Perry, S. R. Marder and J. L. Brédas, *Adv. Funct. Mater.,* 2002, **12**, 631-641.
39 X. Wang, D. M. Nguyen, C. O. Yanez, L. Rodriguez, H. Y. Ahn, M. V. Bondar and K. D. Belfield, *J. Am. Chem. Soc.,* 2010, **132**, 12237–12239.
40 K. D. Belfield, M. V. Bondar, A. R. Morales, X. Yue, G. Luchita and O. V. Przhonska, *J. Phys. Chem. C*, 2012, **116**, 11261−11271.
41 K. D. Belfield, M. V. Bondar, S. Yao, I. A. Mikhailov, V. S. Polikanov and O. V. Przhonska, *J. Phys. Chem. C*, 2014, **118**, 13790–13800.
42 L. Ma, Z. Wu, G. Zhou, F. Yuan, Y. Yu, C. Yao, S. Ning, X. Hou, Y. Li, S. Wang and Q. Gong, *J. Mater. Chem. C*, 2015, **3**, 7004-7013.
43 J.-C. Ribierre, L. Zhao, M. Inoue, P.-O. Schwartz, J.-H. Kim, K. Yoshida, A. S. D. Sandanayaka, H. Nakanotani, L. Mager, S. Méry and C. Adachi*, Chem. Commun.*, 2016, **52**, 3103–3106.
44 K. D. Belfield, M. V. Bondar, H. S. Haniff, I. A. Mikhailov, G. Luchita and O. V. Przhonska, *ChemPhysChem.,* 2013, **14**, 3532-3542.
45 K. M. Shafeekh, S. Das, C. Sissa and A. Painelli, *J. Phys. Chem. B,* 2013, **117**, 8536-8546
46 C. Katan, M. Charlot, O. Mongin, C. Le Droumaguet, V. Jouikov, F. Terenziani, E. Badaeva, S. Tretiak and M. Blanchard-Desce, *J. Phys. Chem. B,* 2010, **114**, 3152−3169.
47 G. Ponterini, D. Vanossi and F. Momicchioli*, Phys. Chem. Chem. Phys.*, 2012, **14**, 4171−4180.
48 F. Todescato, I. Fortunati, S. Carlotto, C. Ferrante, L. Grisanti, C. Sissa, A. Painelli, A. Colombo, C. Dragonetti and D. Roberto, *Phys. Chem. Chem. Phys.,* 2011, **13**, 11099−11109.
49 C. Sissa, A. Painelli, M. Blanchard-Desce and F. Terenziani, *J. Phys. Chem. B,* 2011, **115**, 7009–7020.
50 C. Sissa, V. Calabrese, M. Cavazzini, L. Grisanti, F. Terenziani, S. Quici and A .Painelli, *Chem. Eur. J.,* 2013, **19**, 924−935.
51 A. Painelli, *Chem. Phys.,* 2000, **253**, 393.